

Supporting Information

Decisive Role of Non-Rare Earth Metal in High-Regioselectivity Addition of μ_3 -Carbido Clusterfullerene

Muqing Chen*, Yaoxiao Zhao, Fei Jin, Mengyang Li, Runnan Guan, Jinpeng Xin, Yangrong Yao, Xiang Zhao*, Guan-Wu Wang*, Qianyan Zhang*, Su-Yuan Xie, Shangfeng Yang*

Table of contents

1. Computational details	S2
2. Separation, purification and mass spectrum of $\text{Dy}_2\text{TiC}@I_h\text{-C}_{80}$	S2
3. Separation and crystal data of $\text{Dy}_2\text{TiC}@I_h\text{-C}_{80}$ and $\text{Dy}_2\text{TiC}@I_h\text{-C}_{80}\text{-Ad}$	S3
4. Theoretical calculations of $\text{Dy}_2\text{TiC}@I_h\text{-C}_{80}$ and $\text{Dy}_2\text{TiC}@I_h\text{-C}_{80}\text{-Ad}$	S6
5. Electrochemical data of $\text{Dy}_2\text{TiC}@I_h\text{-C}_{80}$ and $\text{Dy}_2\text{TiC}@I_h\text{-C}_{80}\text{-Ad}$	S9

1. Computational details.

Gaussian 09 program^[1] was used for all of density functional theory (DFT) calculations. Geometrical optimization without symmetry limitation and frequency computation were performed on the B3LYP/6-31G(d)~CEP-4G for all of endohedral metallofullerenes and their Ad addition derivatives. The CEP-4G basis set for metal atoms and the 6-31G(d) basis set for non-metal atoms were used. All of structures were free from imaginary frequency. Natural bond orbital (NBO) was analyzed on the B3LYP/6-311G(d, p)~CEP-4G. Bond critical point (BCP) was analyzed based on quantum theory of atoms in molecules by Multiwfn program.^[32]

2. Separation, purification and mass spectrum of Dy₂TiC@I_h-C₈₀.

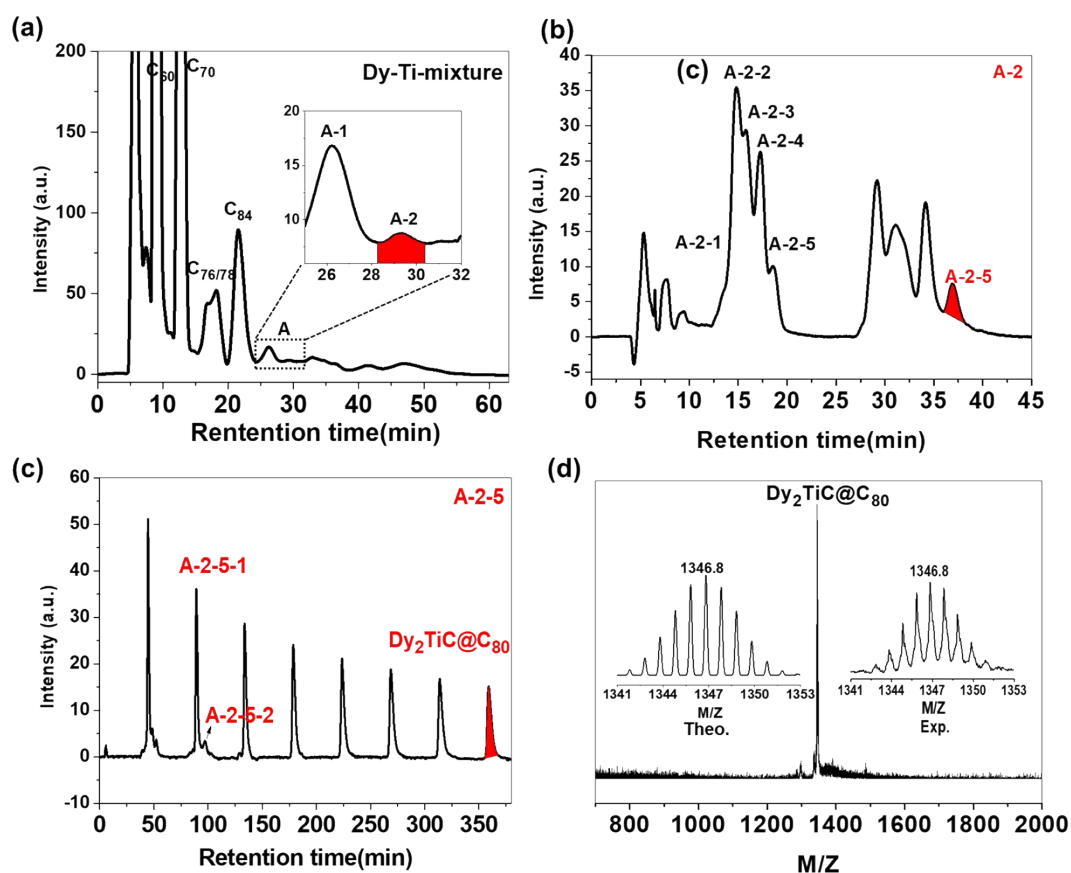


Fig. S1 (a) The HPLC profiles of the raw solution extracted from the carbon soot. Conditions: 5PYE column (20 mm×250 mm); flow rate 15.0 mL min⁻¹; injection volume 15 mL; toluene as the eluent (mobile phase). (b) The HPLC profile of the toluene solution containing Dy₂TiC@I_h-C₈₀ in second-step separation. Conditions: BPM column (10 mm×250 mm); flow rate 5.0 mL min⁻¹; injection volume 5 mL; toluene as the eluent (mobile phase). (c) The recycle HPLC profile of the toluene solution containing Dy₂TiC@I_h-C₈₀ in third-step separation. Conditions: Buckyprep column (20 mm×250 mm); flow rate 15.0 mL min⁻¹; injection volume 15 mL; toluene as the eluent (mobile phase). (d) MALDI-TOF mass spectrum of Dy₂TiC@I_h-C₈₀.

3. Separation and crystal data of $\text{Dy}_2\text{TiC}@I_h\text{-C}_{80}$ and $\text{Dy}_2\text{TiC}@I_h\text{-C}_{80}\text{-Ad}$.

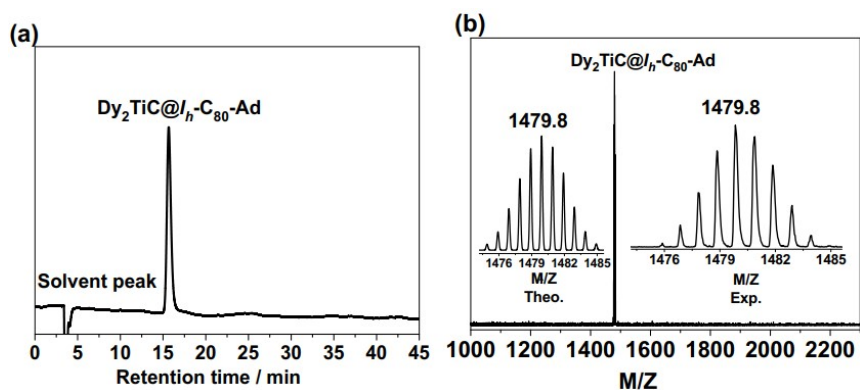


Fig. S2 (a) HPLC profile of the pure $\text{Dy}_2\text{TiC}@I_h\text{-C}_{80}\text{-Ad}$. Conditions: Buckyprep column (\varnothing 4.6 mm \times 250 mm), 20 μL injection volume, 1.0 mL min^{-1} toluene flow, RT, λ = 330 nm UV detector; (b) MALDI-TOF mass spectrum of $\text{Dy}_2\text{TiC}@I_h\text{-C}_{80}\text{-Ad}$.

Table S1. Crystal data of Dy₂TiC@I_h-C₈₀ and Dy₂TiC@I_h-C₈₀-Ad.

Crystal	2DPC· {Dy ₂ TiC@I _h -C ₈₀ }	4DPC· 2{Dy ₂ TiC@I _h -C ₈₀ -Ad}
Empirical formula	C ₂₂₉ H ₁₁₂ Dy ₂ N ₂₀ Ti	C ₄₅₀ H ₂₂₁ Dy ₄ N ₄₀ Ti ₂
Formula weight	3516.28	6933.45
Crystal system	monoclinic	monoclinic
Space group	<i>P2₁/c</i>	<i>P2₁/c</i>
a, Å	14.719	55.239
b, Å	31.919	14.664
c, Å	32.098	39.306
α, deg	90	90
β, deg	101.42	101.38
γ, deg	90	90
Volume, Å ³	14781.6	31212.9
Z	4	4
T, K	100(2)	100(2)
Radiation (λ, Å)	synchrotron (λ = 0.71073)	synchrotron (λ = 0.71073)
ρ _{calc} , g/cm ³	1.580	1.475
μ/mm ⁻¹	1.130	1.069
F(000)	7120.0	14036
Unique data (R _{int})	20725	54668
Parameters	2435	5330
Restraints	351	2499
Observed data (I ≥ 2σ(I))	20725	54668
R ₁ (reflections with I > 2σ(I))	0.0712	0.0764
wR ₂ (all data)	0.2054	0.2282

Table S2. Disorder and occupancy of endohedral metal atoms including Ti^{4+} , Dy^{3+} within $\text{Dy}_2\text{TiC}@I_h\text{-C}_{80}$ and $\text{Dy}_2\text{TiC}@I_h\text{-C}_{80}\text{-Ad}$.

$\mu_3\text{-CCFs}$	Disorder and Occupancy	
$\text{Dy}_2\text{TiC}@I_h\text{-C}_{80}$	Ti, four disorders	Ti1(Ti), 0.80; Ti2, 0.10; Ti3, 0.07; Ti4, 0.03
	Dy1, four disorders	Dy1, 0.91; Dy2B, 0.06; Dy3B, 0.02; Dy4B, 0.01
	Dy2, four disorders	Dy2, 0.82; Dy2A, 0.03; Dy3A, 0.03; Dy4A, 0.12
$\text{Dy}_2\text{TiC}@I_h\text{-C}_{80}\text{-Ad}$	Ti, without disorder	Ti, 1.00
	Dy1, five disorders	Dy1B(Dy1), 0.42; Dy2B, 0.18; Dy3B, 0.04; Dy4B, 0.29; Dy5B, 0.07
	Dy2, four disorders	Dy1A(Dy2), 0.43; Dy2A, 0.07; Dy3A, 0.20; Dy4A, 0.30

Table S3. The crystal structure information of $\text{Dy}_2\text{TiC}@I_h\text{-C}_{80}$ and $\text{Dy}_2\text{TiC}@I_h\text{-C}_{80}\text{-Ad}$.

Bond type	$\text{Dy}_2\text{TiC}@I_h\text{-C}_{80}$		$\text{Dy}_2\text{TiC}@I_h\text{-C}_{80}\text{-Ad}$	
	Bond length (Å)		Bond length (Å)	
Ti- $\text{C}_{\text{cluster}}$	Ti-C81	1.82	Ti-C81	1.83
	Ti-C1	2.26	Ti-C1	2.29
Ti- C_{cage}	Ti-C2	2.13	Ti-C2	2.29
	Ti-C3	2.17	Ti-C3	2.34
Dy1- $\text{C}_{\text{cluster}}$	Dy1-C81	2.14	Dy1-C81	2.23
Shortest Dy1- C_{cage}	Dy1-C47	2.34	Dy1-C37	2.30
Dy2- $\text{C}_{\text{cluster}}$	Dy2-C81	2.17	Dy2-C81	2.14
Shortest Dy2- C_{cage}	Dy2-C75	2.39	Dy2-C59	2.28

4. Theoretical calculations of Dy₂TiC@I_h-C₈₀ and Dy₂TiC@I_h-C₈₀-Ad.

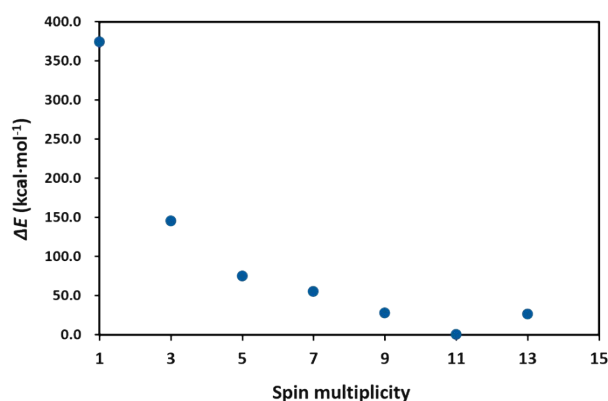


Fig. S3 The relative energy (ΔE) of Dy₂TiC@I_h-C₈₀ with various spin multiplicities.

Dy₂TiC@I_h-C₈₀ with various spin multiplicities were optimized. As shown in Fig. S4, possessing the lowest relative potential energy, $S = 5$ spin ground state was identified for Dy₂TiC@I_h-C₈₀. The optimized geometry of ground-state Dy₂TiC@I_h-C₈₀ was extremely similar with the crystallographic geometry. Specifically, there were same positions ([5, 6]-bond around Ti and hexagon around Dy) of metals and similar bond lengths between metals and inner C_{cluster} atom. Notably, the theoretical bond length (1.79 Å) of Ti-C in Dy₂TiC was slightly shorter than the experimental one (1.82 Å) with obvious double-bond character of Ti-C in inner cluster. To further dissect the electronic configurations and bonding features of Dy₂TiC@I_h-C₈₀, natural electron populations including α and β electron populations on metals are given in Table S4 via Natural Bond Orbital (NBO) analysis. Compared with the valence electron configuration of $4f^{10}6s^2$ for ground-state Dy atom, the Dy³⁺ with five unpaired electrons on each Dy was inferred, which accorded with the $S = 5$ ground state and was also confirmed by the exclusively electronic spin density on Dy atoms in Dy₂TiC@I_h-C₈₀ (Fig. S5c). No electronic spin density on Ti atom indicated that the bonding or transferring of valence electrons for Ti in Dy₂TiC@I_h-C₈₀. The double bond (Fig. S5a and S5b) between Ti and C within the encapsulated Dy₂TiC cluster in Dy₂TiC@I_h-C₈₀ was confirmed with Mayer bond order (MBO) of 1.96 and Wiberg bond order (WBO) of 2.18 (Table S5), which was in line with the double-bond speculation based on the bond length between Ti and C in experiment. It could be found that the d orbitals of Ti mainly contributed to this double bond (Fig. S5a and S5b). Furthermore, according to the NBO analysis (Table S4), there is no electron on 4s of Ti, then Ti⁴⁺ can be deduced in Dy₂TiC@I_h-C₈₀. Thus, a formal electronic configuration of [(Dy³⁺)₂Ti⁴⁺C⁴⁺]⁶⁺@[I_h-C₈₀]⁶⁻ is inferred, which accorded with the general six-electron transfer from the encapsulated cluster to the outer fullerene cages for trimetallic nitride clusterfullerenes (NCFs).²⁻⁴ Similarly, Ti⁴⁺ and Dy³⁺ were also found in Dy₂TiC@I_h-C₈₀-Ad. As shown in Table S5, except for the double bond between Ti and C, it could be seen that there were single bonds between Dy and C in Dy₂TiC@I_h-C₈₀ and Dy₂TiC@I_h-C₈₀-Ad (Table S5).

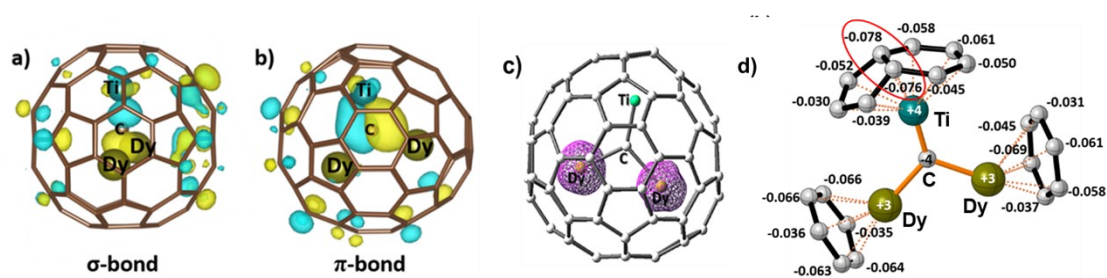


Fig. S4 (a) σ -bond and (b) π -bond of Ti-C_{cluster} for Dy₂TiC@I_h-C₈₀; (c) electronic spin density of Dy₂TiC@I_h-C₈₀. (Isovalue = 0.004 au); (d) charges of C close to metals of Dy₂TiC@I_h-C₈₀ on B3LYP/6-311G(d, p)-CEP-4G level. The red circle highlights the carbon atoms with highest electronic density.

Table S4. Natural electron population of metals in Dy₂TiC@I_h-C₈₀.^a

Dy ₂ TiC@I _h -C ₈₀	α -electron population	β -electron population
Ti	$3d^{1.10}4p^{0.23}4d^{0.11}5s^{0.07}$	$3d^{1.11}4p^{0.23}4d^{0.12}5s^{0.06}$
Dy2	$4f^{7.00}5d^{0.54}6s^{0.05}6p^{0.09}6d^{0.01}7p^{0.06}$	$4f^{2.05}5d^{0.49}6s^{0.05}6p^{0.08}6d^{0.01}7p^{0.06}$
Dy1	$4f^{7.00}5d^{0.54}6s^{0.05}6p^{0.09}6d^{0.01}7p^{0.06}$	$4f^{2.06}5d^{0.50}6s^{0.05}6p^{0.08}6d^{0.01}7p^{0.06}$

^a Although there were respectively $3d^{1.10}$ and $3d^{1.11}$ in α - and β -electron population for Ti, Ti⁴⁺ was evidently inferred in Dy₂TiC@I_h-C₈₀ because the electron population in every α - or β -orbital of $3d$ was less than 0.28 for Ti.

Table S5. Bond length (L, in Å), MBOs and WBOs between the center C and metals (Ti and Dy) for Dy₂TiC@I_h-C₈₀ and Dy₂TiC@I_h-C₈₀-Ad.

□	Dy ₂ TiC@I _h -C ₈₀			Dy ₂ TiC@I _h -C ₈₀ -Ad		
	L (Å)	MBO	WBO	L(Å)	MBO	WBO
Ti-C81	1.7927	1.96	2.18	1.8121	1.91	2.21
Dy2-C81	2.1826	0.69	0.86	2.2306	0.72	0.83
Dy1-C81	2.1741	0.71	0.89	2.2173	0.72	0.86

Table S6. Bond critical point (BCP) parameters and MBOs of Dy₂TiC@I_h-C₈₀.

Bond	distance/Å	ρ_{BCP}^a	$\nabla^2\rho_{\text{BCP}}^a$	MBO
Ti-C2	2.14	0.0716	0.2507	0.28
Ti-C3	2.38	0.0754	0.2634	0.26
Dy1-C47	2.39	0.0603	0.1900	0.18
Dy2-C75	2.44	0.0553	0.1776	0.18

^a ρ_{BCP} is the density of all electrons and $\nabla^2\rho_{\text{BCP}}$ is the Laplacian of the electron density.

Table S7. Total MBOs between the I_h-C₈₀ cage and Ti or Dy for Dy₂TiC@I_h-C₈₀ and Dy₂TiC@I_h-C₈₀-Ad.

	Dy ₂ TiC@I _h -C ₈₀	Dy ₂ TiC@I _h -C ₈₀ -Ad
Ti-Cage	2.70	2.86
Dy2-Cage	2.09	2.11
Dy1-Cage	2.07	2.06

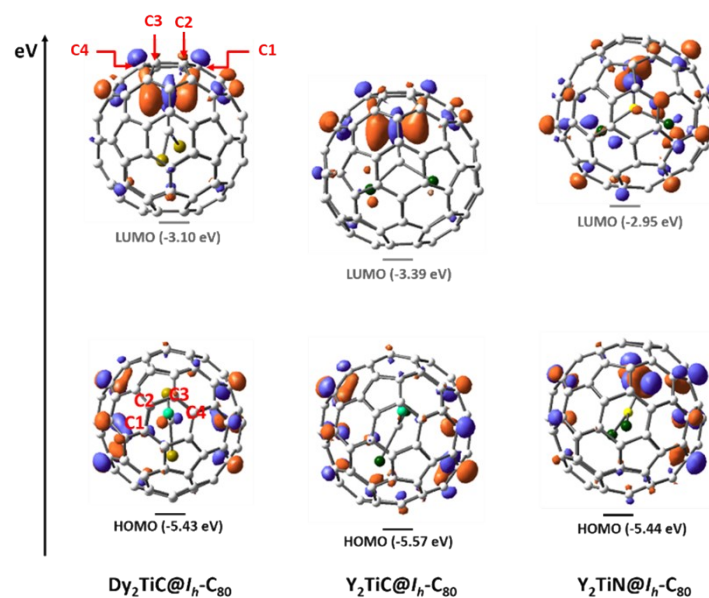


Fig. S5 Frontier molecular orbital diagrams (isosurface = 0.04 au) of $\text{Dy}_2\text{TiC}@I_h\text{-C}_{80}$, $\text{Y}_2\text{TiC}@I_h\text{-C}_{80}$, and $\text{Y}_2\text{TiN}@I_h\text{-C}_{80}$.

5. Electrochemical data of $\text{Dy}_2\text{TiC}@I_h\text{-C}_{80}$ and $\text{Dy}_2\text{TiC}@I_h\text{-C}_{80}\text{-Ad}$.

Table S8. Redox potentials (half-wave potential, V vs Fc^+/Fc) of $\text{Dy}_2\text{TiC}@I_h\text{-C}_{80}$ and $\text{Dy}_2\text{TiC}@I_h\text{-C}_{80}\text{-Ad}$ in comparison with those of $\text{M}_3\text{N}@C_{80}$ ($\text{M} = \text{Sc}, \text{Lu}$) nitride clusterfullerenes.

Compound	ox E_2	ox E_1	red E_1	red E_2	red E_3	Ref.
$\text{Dy}_2\text{TiC}@I_h\text{-C}_{80}$	1.01	0.57	-0.93	-1.62	-1.81 ^a	This work
$\text{Dy}_2\text{TiC}@I_h\text{-C}_{80}\text{-Ad}$	0.97 ^a	0.49	-1.10 ^a	-1.58 ^a	-1.83 ^a	This work
$\text{Sc}_3\text{N}@I_h\text{-C}_{80}$	-	0.65	-1.07 ^a	-1.46 ^a	-1.78 ^a	3
$\text{Sc}_3\text{N}@I_h\text{-C}_{80}\text{-Ad}$ (2a)	-	0.58	-1.15	-1.59	-1.89	3
$\text{Sc}_3\text{N}@I_h\text{-C}_{80}\text{-Ad}$ (2b)	-	0.57	-1.08	-	-	3
$\text{Lu}_3\text{N}@I_h\text{-C}_{80}$	-	0.61	-1.41	-1.91	-2.56	3
$\text{Lu}_3\text{N}@I_h\text{-C}_{80}\text{-Ad}$ (3a)	-	0.50	-1.57	-2.08	-2.73	3
$\text{Lu}_3\text{N}@I_h\text{-C}_{80}\text{-Ad}$ (3b)	-	0.52	-1.48	-2.15	-	3

^a peak potential (irreversible redox process).

References

1. M. J. Frisch, G. W. Trucks, H. B. Schlegel, G. E. Scuseria, M. A. Robb, J. R. Cheeseman, G. Scalmani, V. Barone, B. Mennucci, G. A. Petersson, et al., Gaussian 09, Gaussian, Inc., Wallingford, CT, USA, 2009.
2. T. Lu, F. W. Chen, *J. Comput. Chem.* **2012**, *33*, 580-592.
3. M. Yamada, T. Abe, C. Saito, T. Yamazaki, S. Sato, N. Mizorogi, Z. Slanina, F. Uhlík, M. Suzuki, Y. Maeda, Y. Lian, X. Lu, M. M. Olmstead, A. Balch, S. Nagase, T. Akasaka, *Chem. Eur. J.* **2017**, *23*, 6552-6561.